

Analysis, manufacture and characterization of Ni/Cu functionally graded structures

Wilfredo Montealegre Rubio^{a,*}, Glaucio H. Paulino^{b,c}, Emilio Carlos Nelli Silva^d

^aSchool of Mechatronic, Faculty of Mines, Universidad Nacional de Colombia, Carrera 80 No. 65-223, bloque M8, oficina 113, Medellín, Antioquia, Colombia

^bNewmark Laboratory, Department of Civil and Environmental Engineering, University of Illinois at Urbana–Champaign, 205 North Mathews Av., Urbana, IL 61801, USA

^cDepartment of Mechanical Science and Engineering, University of Illinois at Urbana–Champaign, 158 Mechanical Engineering Building, 1206 West Green Street, Urbana, IL 61801-2906, USA

^dDepartment of Mechatronics and Mechanical Systems Engineering, Escola Politécnica da Universidade de São Paulo, Av. Prof. Mello Moraes, 2231 – Cidade Universitária, São Paulo, SP 05508-900, Brazil

ARTICLE INFO

Article history:

Received 8 February 2012

Accepted 20 April 2012

Available online 26 April 2012

Keywords:

A. Functionally graded structures

C. Spark plasma sintering

A. Nickel/copper gradation

ABSTRACT

In this work, an experimental and numerical analysis and characterization of functionally graded structures (FGSs) is developed. Nickel (Ni) and copper (Cu) materials are used as basic materials in the numerical modeling and experimental characterization. For modeling, a MATLAB finite element code is developed, which allows simulation of harmonic and modal analysis considering the graded finite element formulation. For experimental characterization, Ni–Cu FGSs are manufactured by using spark plasma sintering technique. Hardness and Young's modulus are found by using microindentation and ultrasonic measurements, respectively. The effective gradation of Ni/Cu FGS is addressed by means of optical microscopy, energy dispersive spectrometry, scanning electron microscopy and hardness testing. For the purpose of comparing modeling and experimental results, the hardness curve, along the gradation direction, is used for identifying the gradation profile; accordingly, the experimental hardness curve is used for approximating the Young's modulus variation and the graded finite element modeling is used for verification. For the first two resonance frequency values, a difference smaller than 1% between simulated and experimental results is obtained.

© 2012 Elsevier Ltd. All rights reserved.

1. Introduction

Functionally graded materials (FGMs) are composite materials whose properties are continuously graded along a specific material direction. The property change is generally obtained through continuous change of material microstructure [1], see Fig. 1. In some graded structures, the volume fraction of one of the phases varies continuously between 0% and 100%, between two points of the structure; for instance, in Fig. 1, the material A is gradually replaced by material B, leading to a composite material with the volume fraction of material A and material B varying smoothly through a transition zone [2–4].

One advantage of such FGM structures is the possibility of taking advantage of material properties of each base material. For example, by combining metal/ceramic constituents, one can design a thermal barrier on one side, which has the thermal properties of ceramic materials and, a metallic material on the opposite side, which has high tensile strength and toughness. Thus, the graded structure takes advantage of each base material without conventional material interfaces [5]. The absence of such material

interfaces offers other interesting local features: (i) local reduction of residual thermal stress, and (ii) redistribution of mechanical stresses, which may arise from the difference in stiffness between phases [6,7].

Two approaches can be followed for modeling FGM: analytical and numerical. In the first approach, solutions are usually obtained for simplified problems (with simple boundary conditions and/or initials), due to the difficulty of faithfully representing all the microstructure details inherent in this kind of problem; specifically, to model the shape, size and continuous material distribution at each Cartesian coordinate [8,9]. Therefore, FGM modeling has been addressed by using numerical analysis, including, homogenization methods. The homogenization methods are based on the periodicity of a base cell or Representative Volume Element (RVE) [10] or statistical homogeneity of the composite [11]. Other modeling studies address FGM plates, in dynamic analysis, using shear deformation plate theories and non-linear von Karman theory [12,13], or simulate the wave propagation in graded piezoelectric [14] and graded non-piezoelectric materials [15] by using the spectral finite element method, or simulate FGM structures, in dynamic analysis, with the traditional finite element by using commercial software such as ADINA [16] and ANSYS [17]. Finally, new finite elements have been formulated considering the material gradation inside the element, which is called the Graded Finite

* Corresponding author. Tel.: +57 4 4255267/4255260.

E-mail addresses: wmontealegrer@unal.edu.co (W.M. Rubio), paulino@illinois.edu (G.H. Paulino), ecnsilva@usp.br (E.C.N. Silva).

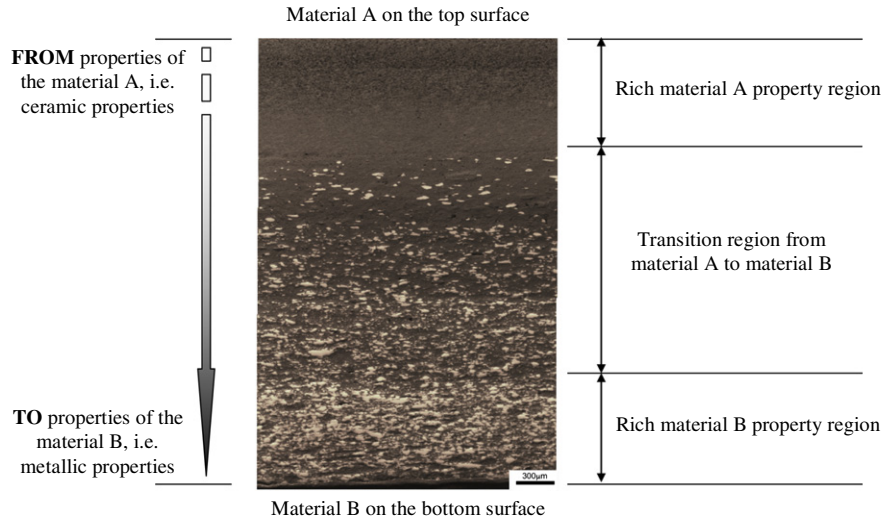


Fig. 1. Illustration of the FGM concept by means of a microphotography for a PZT-5A/Ni FGM [46].

Element (GFE) formulation [18–20]. In GFE formulation, the material gradation is incorporated at finite element scale, which results in a continuous and smooth property material variation between elements. The GFE formulation has been applied to static structural problems [18,19], dynamic structural problems [21,22] and static and dynamic piezoelectric problems [17,23].

Some experimental works have concentrated on characterizing the structural behavior of graded structures when subjected to dynamic loads [24–27], or on manufacturing FGM based on the combination of different materials [28,29]. However, this list of references is not representative, and thus the reader is referred to the technical literature in the field (e.g. Experimental Mechanics journal).

In this work, a comparison between experimental and numerical frequency response is performed (simulated by means of the GFE formulation) for a nickel/copper functionally graded structure (Ni/Cu FGS), which is manufactured by using Spark Plasma Sintering (SPS) technique. Through this comparison, the use of the hardness curve, along the gradation direction, for estimating the elastic property gradation function in isotropic and completely solid miscible materials, is addressed. In addition, in order to determine the effective gradation, Ni/Cu FGSs are comprehensively characterized, which includes optical and scanning electron microscopy, energy dispersive spectrometry (EDS), and hardness testing.

The paper is organized as follows. First, the GFE formulation, implemented in MATLAB™ code, is presented (Section 2). Next, in Sections 3 and 4, the manufacturing and characterization of Ni/Cu are respectively shown. Finally, the methodology used to validate the Ni/Cu FGS results is presented (Section 5) and some conclusions are inferred (Section 6).

2. The graded finite element formulation in harmonic analysis

In this work, the harmonic response obtained by a finite element program based on the GFE formulation [18,19] is implemented. In harmonic analysis, a continuous sine excitation is assumed as input and the response with this signal type, at different frequencies, is performed. In other words, the harmonic analysis looks for the response amplitude, in steady state, when the prescribed loads vary periodically. So, the following equation (without considering damping) is solved:

$$(-\Omega_c^2 \mathbf{M} + \mathbf{K}) \mathbf{u}_0 = \mathbf{F}_0 \quad (1)$$

where the term \mathbf{F}_0 is the mechanical load amplitude given by [30]:

$$\mathbf{F}_p = \mathbf{F}_0 \exp(-j\Omega_c t) \quad (2)$$

in which Ω_c is the circular frequency of the input signal, and \mathbf{M} and \mathbf{K} represent the mass and stiffness matrices, respectively. The term t represents time and $j = \sqrt{-1}$. The term \mathbf{u}_0 is the displacement amplitude, which assumes that its general solution is expressed as [30]:

$$\mathbf{u} = \mathbf{u}_0 \exp(-j\Omega_c t) \quad (3)$$

For each circular frequency of the excitation input, an equivalent problem must be solved, as follows:

$$\bar{\mathbf{K}} \mathbf{u}_0 = \mathbf{F}_0 \quad \text{with:} \quad \bar{\mathbf{K}} = -\Omega_c^2 \mathbf{M} + \mathbf{K} \quad (4)$$

Additionally, the mass and stiffness matrices, of each finite element, are expressed as:

$$\mathbf{M}^e = \iint \mathbf{N}^T \rho^e(x, y) \mathbf{N} dx dy \quad \text{and} \quad \mathbf{K}^e = \iint \mathbf{B}^T \mathbf{E}^e(x, y) \mathbf{B} dx dy \quad (5)$$

where the terms \mathbf{N} and \mathbf{B} represent the usual shape functions and the displacement–strain matrix, respectively. Integrals in Eq. (5) are developed over finite element e . Properties ρ and \mathbf{E} represent the density and elastic matrix, respectively. The material properties depend on Cartesian position: coordinates x and y in a bi-dimensional analysis.

To treat the continuous material gradation in relation to the Cartesian coordinates, the GFE formulation is adopted [22]. Fig. 2 compares the traditional Homogeneous Finite Element (HFE) formulation with the GFE formulation. In HFE case, the material properties remain constant within the finite element; see Fig. 2a, and they are evaluated at the centroid of each element. Because the GFE incorporates the material property gradation on the finite element scale, see Fig. 2b, the properties inside each element change following a specific gradation pattern or function. Accordingly, property “transition” from a finite element to another is smooth and continuous, without “jumps” from element to element. Hence, the GFE formulation is a more “natural” way for simulating the property variation in an FGS.

To accomplish continuous property change in an FGS, element properties are evaluated by interpolation functions, which are based on the nodal property values according to the Generalized Isoparametric Formulation (GIF) [18]. In this work, the same functions for interpolating the geometry and displacement are also used for interpolating the material properties. Thus, the density and elastic matrix properties are respectively expressed, for each finite element e , as:

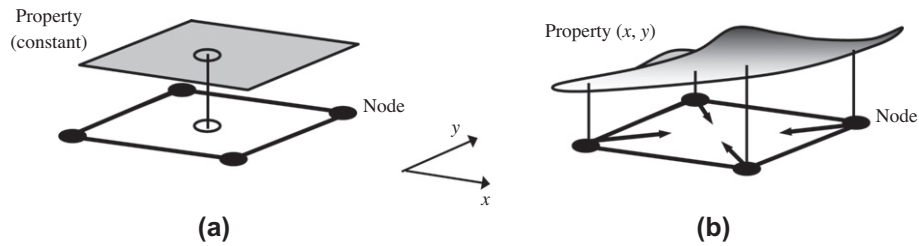


Fig. 2. Material property distribution in: (a) homogeneous finite element; (b) graded finite element.

$$\rho = \sum_{n=1}^{n=n_d} N_n \rho_n \quad \text{and} \quad \mathbf{E}^e = \sum_{n=1}^{n=n_d} N_n \mathbf{E}_n \quad (6)$$

where n_d is the number of nodes per finite element. Terms ρ_n and \mathbf{E}_n represent density and elastic matrix properties per node n respectively. The material properties (see Eq. (5)) must be properly integrated. By contrast, in the HFE formulation, these properties are usually constant. A computer code has been implemented in MATLAB.

3. Manufacturing of Ni/Cu FGS

The Spark Plasma Sintering (SPS) technique is a sintering process with simultaneous application of low voltages, high current density pulses, and applied uniaxial pressure [31,32]. Fig. 3a shows the configuration of the SPS system used in the present research. In sintering, “green” samples or non-sintered samples are placed inside a graphite die, in a vacuum chamber, where graphite electrodes act as a mechanism for vertically pressurizing the samples. By applying voltage pulses with high direct electrical current to the graphite die, high temperatures are achieved, which promote the material densification. In addition, material diffusion is promoted by application of uniaxial pressure [32]. Fig. 3b shows the SPS machine used in the Laboratory of Sensors and Actuators of the Polytechnic School of the University of São Paulo, which is based on the configuration shown in Fig. 3a.

In this work, nickel (Ni) and copper (Cu) are employed as raw materials. Although several previous studies have dealt with SPS manufacturing of Cu compounds [33,34] or nickel/alumina FGS [35] and nickel/titanium FGS [29], here we deal with only Ni/Cu material combination as base material of FGS. In this case, the

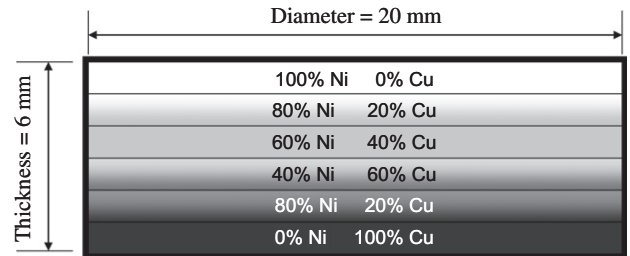


Fig. 4. Green layer configuration before sinterization including material percentage by layer.

near-optimal sintering temperature of the resulting functionally graded material is obtained because the sintering temperature of both reference materials is close, around 900–1000 °C for nickel [35] and 700–800 °C for copper [33].

Green samples are composed of six layers (approximately 1 mm each), varying in composition along the thickness, as shown in Fig. 4. In addition, a 5 kN pre-compaction axial load is applied to each green layer. Sample dimensions correspond to a 20 mm (diameter) × 6 mm (thickness) disk.

The history curves for the main variables during the sintering process (electric current, pressure and temperature) are shown in Fig. 5. From Fig 5a it is noted that there is a gradual electric current increase to reach the maximum value of 2000 A at 420 s, which corresponds to 82% of the sintering temperature (see Fig. 5b). The current value is stabilized around 1250 A, during the maintenance period of the sintering temperature (with axial pressure of 50 MPa or axial loading of 15.7 kN, for a 20 mm diameter sample, see Fig. 5c). Finally, for cooling the sample and finishing the

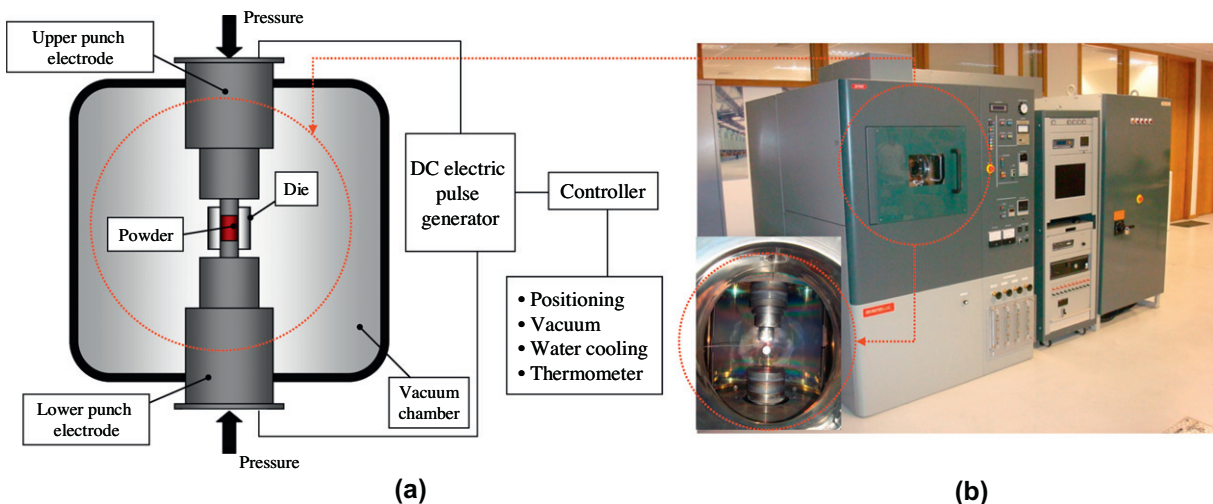


Fig. 3. (a) Typical configuration of SPS technique; (b) Dr. SINTER SPS machine at Polytechnic School of the University of São Paulo.

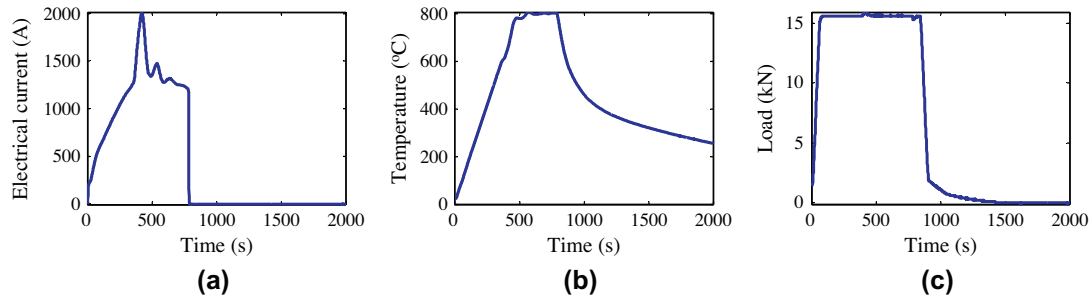


Fig. 5. Curves during sinterization of Ni/Cu FGS: (a) electrical current, (b) temperature and (c) applied axial load.

sintering process, the electric current drops rapidly to zero. The temperature curve shows a gradual cooling, which is generated by heat exchange between the graphite mold and the vacuum chamber. When the sample is taken out from the SPS machine, its temperature is 255 °C (at 2000 s). In general, pressure and temperature curves follow the original pattern.

Fig. 6 shows a Ni/Cu sample, which is manufactured by the SPS technique. It is observed that material gradation is obtained both on the outer and inner (center) surfaces of the disk; however, this gradient does not seem to be uniform along the radial direction because the powder material cannot be completely mixed at each green layer and there is a temperature gradient from the outer surface to the center, which generates different material diffusion rates. However, as shown in the following section (Section 4), powder compaction and an effective property gradient are achieved.

4. Experimental characterization of Ni/Cu FGS

This section presents the methodology used to characterize the Ni/Cu samples. Four Ni/Cu samples are manufactured by using spark plasma sintering following the parameters shown in Fig. 5. Some of the samples are used in destructive testing. Tests consist of: (i) characterization of the microstructure and chemical composition by using a Scanning Electron Microscope (SEM); and (ii) determination of material properties such as Young's modulus, density and hardness aiming at finding the gradation profile of such properties.

4.1. Microstructure and chemical composition characterization

Before being taken to the microscope, two samples are cut in half (by using a precision cutter Isomet 4000 BUEHLER) and are

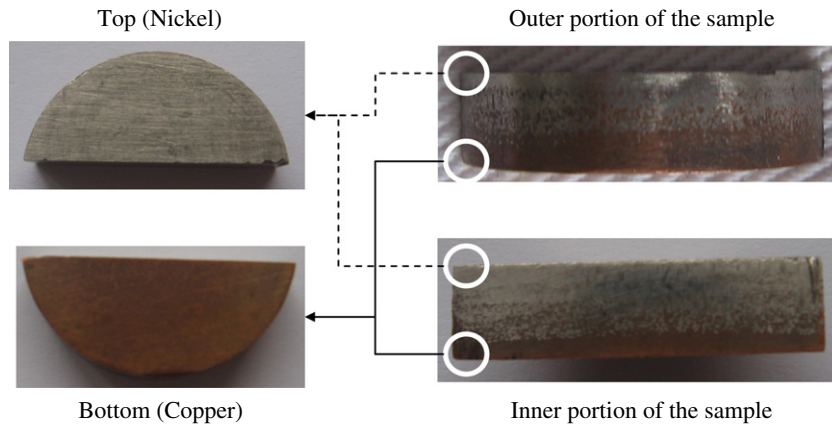


Fig. 6. Ni/Cu FGS sample manufactured by using the SPS technique.

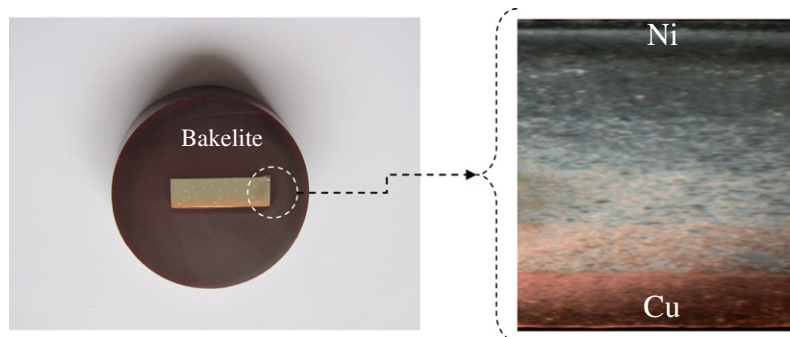


Fig. 7. Left: half of a Ni/Cu FGS sample embedded in Bakelite; right: optical micro photography of material gradation.

embedded in a Bakelite structure, so they can be prepared for subsequent observation. One half-sample is presented in Fig. 7. Subsequently, the free half-surface is polished, including electrolytic polishing. Fig. 7 also shows an image obtained by using an optical microscope OM BX60 OLYMPS. The continuous microstructure gradation is observed, from copper (upper surface of the figure) to nickel. Yellow regions represent areas with the highest concentration of copper particles and gray regions with the highest concentration of nickel particles. Additionally, there is no clear evidence of sintering defects or cracks in layer interfaces. Also, the continuous copper phase dispersion in the nickel phase, from the top to bottom surface, is noted. This dispersion is clearer when material gradation is observed by using a Scanning Electron Microscope – SEM (Philips XL-30) at three different points along the gradation direction (see Fig. 8). On the bottom surface (100% Ni area, see Fig. 4), a quasi-homogeneous distribution of Ni grains is achieved, each grain size around 2.5–5 μm in diameter. In the initial green layer area with 80% Ni and 20% Cu (see Fig. 4), copper inclusions in a nickel matrix are observed; however, the Ni grain size is increased, with 8–10 μm in diameter. This effect is due, in part, to the temperature gradient generated along the gradation direction during the sintering process. In addition, copper grains have irregular shape and distribution. This behavior is inverted in relation to the highest copper concentration regions. Thus, in the initial green layer with 20% Ni and 80% Cu, the grain size in the copper matrix array is approximately 9 μm in diameter and nickel inclusions have irregular shape and they are randomly distributed.

On the other hand, by using the technique of Energy Dispersive Spectrometry – EDS [36], the effective property gradation is confirmed. The procedure consists in finding the chemical composition in several regions along the gradation direction. As illustrated by Fig. 9, the chemical composition of each initial green layer is observed; specifically, the chemical composition gradually changes from nickel (Fig. 9a) to copper (Fig. 9f), approximately following the weight proportion of the green structure (see Fig. 4). Furthermore, Fig. 9a and b indicate some oxidation in the highest nickel concentration areas (nickel oxide – NiO), which could be the product of the electrolytic polishing or high sinterization temperature.

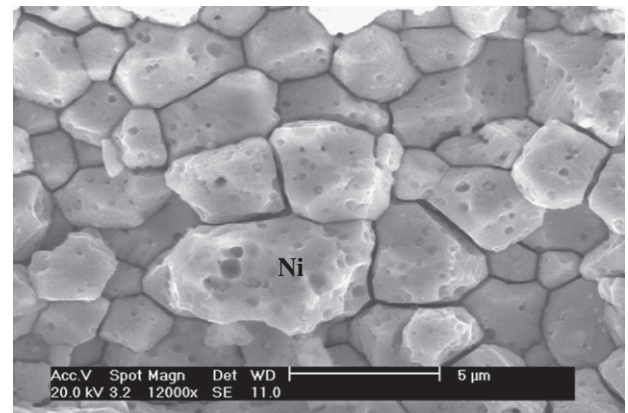
4.2. Determination of hardness, density and Young's modulus

4.2.1. Vickers hardness

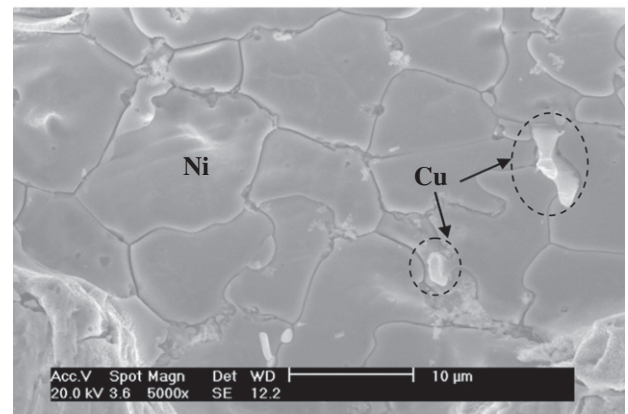
To determine the Vickers hardness along the direction of gradation, a BUEHLER MICROMET 2103 durometer is employed. The hardness is determined for two Ni/Cu FGM samples, which are called Ni/Cu sample 1 and Ni/Cu sample 2, according to ASTM E-384 standard [37]. Three Vickers hardness tests are performed for each area corresponding to the initial green layers, see Fig. 4.

In the 100% Cu region, the Vickers hardness is around 60 kgf/mm². This value increases to around 175 kgf/mm², in the 100% nickel region. These results confirm again that, in fact, the hardness property gradation is achieved (from copper to nickel) along the FGS thickness; however, along the radial direction, the material gradient is not uniform because different Vickers hardness values are obtained along radial direction, see horizontal lines in Table 1. Nevertheless, hardness variation into original green layer remains in relatively small ranges. This variation is probably caused by particle diffusion between green layers during the sintering process, which is not uniform. Particularly, the temperature gradient in the radial direction produces non-uniform mass diffusion.

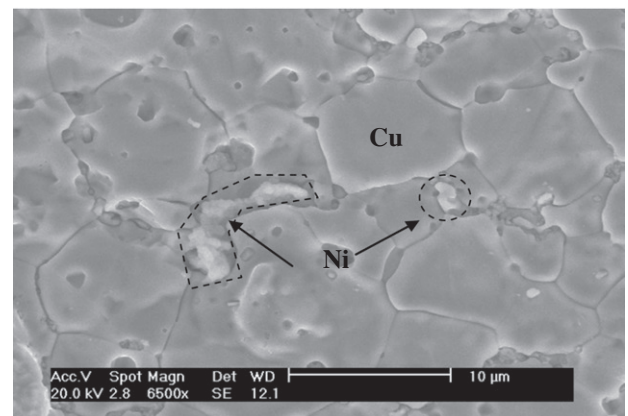
Hardness values shown in Table 1 are used for plotting the average-hardness curve along the gradation direction. This curve is presented in Fig. 10. The hardness changes almost linearly, from 60 Kgf/mm², in the 100% Cu region, to 175 Kgf/mm², in the 100% Ni region.



(a)



(b)



(c)

Fig. 8. SEM microphotography of a Ni/Cu FGS sample at different positions along the gradation direction (according to the schematic illustration of Fig. 4): (a) 100% Ni; (b) 80% Ni, 20% Cu and (c) 20% Ni, 80% Cu.

Several studies have shown that Young's modulus can be estimated by indentation (i.e. from elastic recovery). Oliver and Pharr [38] and Meza et al. [39] have determined the elastic properties of isotropic materials using a nano-hardness instrumented testing; thus, by controlling the loading and the penetration depth of the indenter, the Young's modulus is obtained. Lawn and Howes [40] have estimated the Young's modulus and hardness considering that the elastic recovery extent in the depth of Vickers indentations is related with Young's modulus/hardness ratio. Following a related idea, Marshall et al. [41] have found the relation between

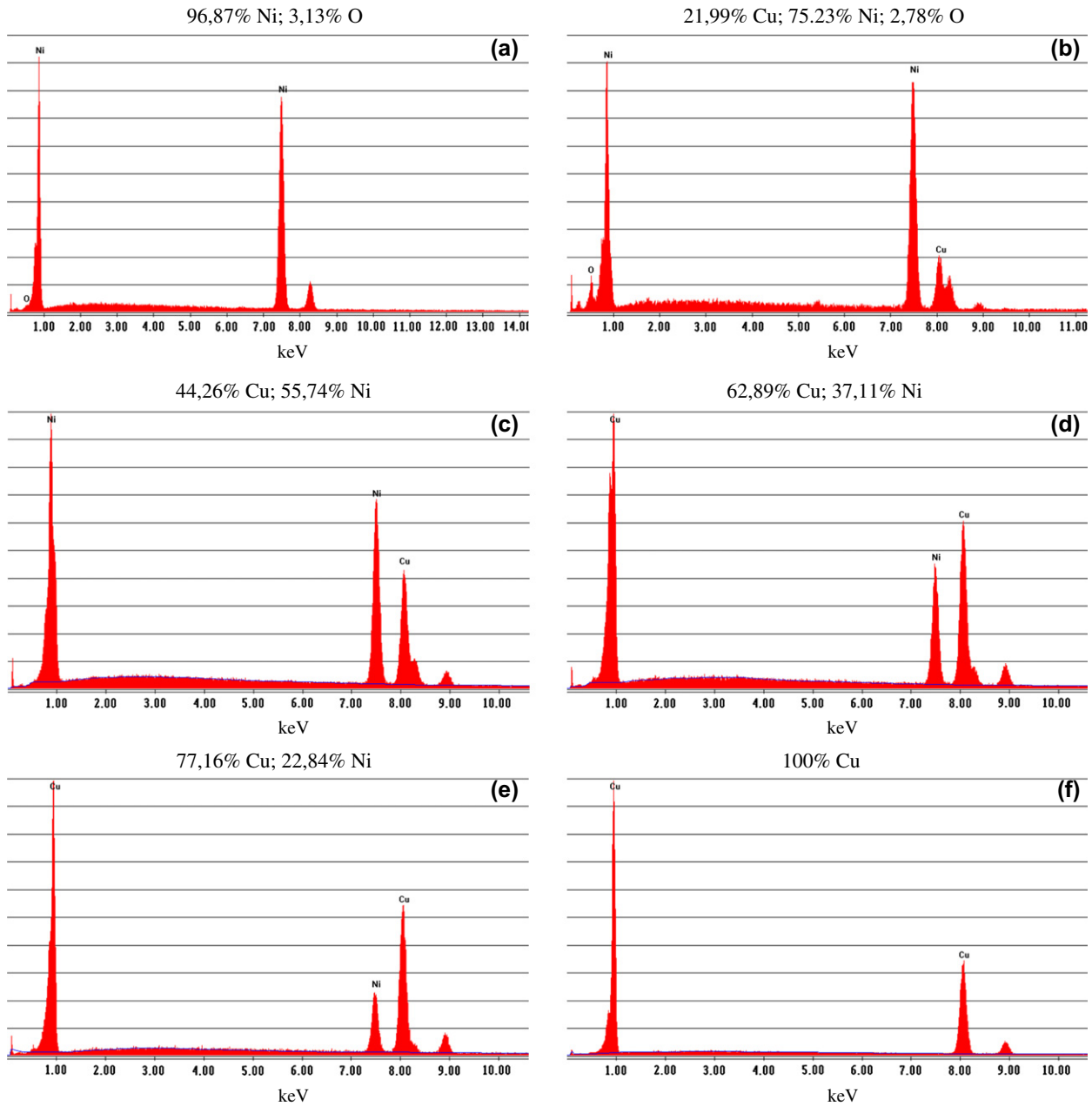


Fig. 9. Chemical composition by using the technique of energy dispersive spectrometry at different positions along the gradation direction according to Fig. 4: (a) 100% Ni; (b) 80% Ni–20% Cu; (c) 60% Ni–40% Cu; (d) 40% Ni–60% Cu; (e) 20% Ni–80% Cu; (f) 100% Cu.

Table 1
Vickers hardness values along thickness direction for Ni/Cu FGS samples.

Layers (%)	Ni/Cu FGS – sample no. 1			Ni/Cu FGS – sample no. 2		
	Measures (kgf/mm ²)			Measures (kgf/mm ²)		
100 Cu	60.9	58.6	59.7	58.4	64.8	69.5
80 Cu, 20 Ni	84.2	83.6	86.1	82.3	83.0	85.0
60 Cu, 40 Ni	106.8	105.3	129.0	120.8	125.8	102.7
40 Cu, 60 Ni	136.6	121.8	120.9	145.3	121.8	119.8
20 Cu, 80 Ni	164.6	163.2	144.4	157.9	133.2	123.7
100 Ni	174.5	173.0	185.3	186.2	160.3	161.1

indentation dimensions and hardness/Young's modulus ratio based on elastic recovery of the in-surface dimensions of a Knoop test. These results led to the assumption that the average-hardness curve (see Fig. 10) can be used, in isotropic and completely solid

miscible materials, as a “pattern” curve, which represents the Young's modulus change along the gradation direction. Before testing this hypothesis (which is presented in Section 5), the Young's modulus in 100% Cu and 100% Ni regions must be determined. Accordingly, the intermediate Young's modulus values can be interpolated following the “pattern” curve (see Fig. 10).

To determine the Young's modulus in 100% Cu and 100% Ni regions, two pure copper and nickel samples are manufactured, by following the same procedure presented in Section 3. Each sample corresponds to a 20 mm in diameter and 6 mm thickness cylinder, each of which is sintered at 800 °C, following temperature and pressure curves shown in Fig. 5.

4.2.2. Bulk density

To determine the density for 100% Cu and 100% Ni samples (non-FGS samples), the volume of each sample is determined by

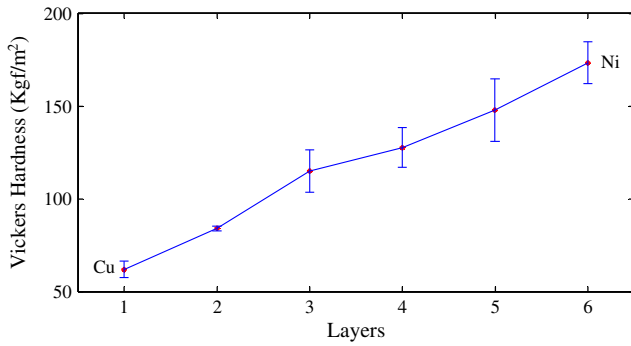


Fig. 10. Vickers-hardness variation curve along gradation direction of Ni/Cu FGS samples. Red points indicate mean value of the hardness values listed at horizontal lines in Table 1. At each point, the error bars also are shown.

Table 2
Density values for copper and nickel samples and other related parameters.

Datum	Non-FGS (only Cu)		Non-FGS (only Ni)	
	Sample 1	Sample 2	Sample 1	Sample 2
Diameter (mm)	19.966	19.874	20.015	20.054
Thickness (mm)	6.051	5.993	5.887	5.964
Mass (gr)	16.179	15.973	16.313	16.133
Density (kg/m ³) – ρ ₁	8539.9	8591.8	8807.2	8564.2
Relative density (%)	95.5	96.1	98.9	96.2

using a micrometer and, by using a precision scale METTLER TOLEDO AB 204 (accurate to 0.0001 g), their mass is measured.

Table 2 summarizes the results of density for each non-FGS sample. Both sets of density measurements provided consistent results. The relative density of samples is higher than 95% when compared to the theoretical density, 8940 kg/m³ for copper C10200 [42] and 8906 kg/m³ for nickel 200 [42]. This shows that there is a powder consolidation during the sintering process; in addition, these results are in agreement with those obtained by Zhang et al. [33], which demonstrate that copper relative density changes according to sinterization parameters, achieving high powder consolidation (relative density exceeding 95%) when the sinterization temperature and pressure are higher than 600 °C and 30 MPa, respectively.

4.2.3. Young’s modulus

The elastic behavior of 100% Cu and 100% Ni samples (non-FGS samples) is determined by measuring the longitudinal wave propagation velocity. Hence, assuming a perfectly elastic material (which satisfies Hooke’s law), Young’s modulus (*E*) is determined by following expression [43]:

$$E = \left[\frac{(1 + \nu)(1 - 2\nu)}{(1 - \nu)} \right] V_l^2 \rho \tag{7}$$

where the terms ρ and *E* are the density and Young’s modulus of the material (nickel or copper), respectively. The term *V_l* is the longitudinal wave propagation velocity, which is determined experimentally. In Eq. (7) is used the theoretical value of the copper and nickel Poisson’s modulus (*ν*).

In this work, the experimental value of *V_l* is determined by using two co-axial piezoelectric transducers, see Fig. 11. One transducer acts as emitter and the other as receiver. Each 100% Cu or 100% Ni sample is placed between the piezoelectric transducers and the elapsed time is measured, since the emitter transducer is excited until receiver catches the propagated wave. Accordingly, by using the propagation wave time along thickness *d* (Fig. 11), the longitudinal wave propagation velocity within the material is calculated.

The experimental setup for measuring the elastic properties by ultrasound technique consists in a 5072PR PANAMETRICS pulser/receiver and two 10 MHz piezoelectric transducers (see Fig. 11). Signals are digitized by a 54820A AGILENT INFINIUM oscilloscope with 8 bits vertical resolution, by using a 500 MHz sampling frequency. Observed signals can be seen in Fig. 12a and b for 100% Cu or 100% Ni samples, respectively.

Table 3 summarizes the results for each 100% Cu or 100% Ni sample: (i) the propagation wave time (*t*) along thickness *d* (thickness of each sample presented in Table 2), (ii) longitudinal wave propagation velocity, which is calculated by *V_l* = 2*d*/*t* and (iii) Young’s modulus values, which are calculated by using Eq. (7).

Table 3 shows that Young’s modulus for all samples is close to theoretical value (pure materials): 113 GPa for copper C10200 [42] and 214 GPa for nickel 200 [42]. The difference is due to the fact that, in the SPS, pure copper and nickel are not used, which increases the losses by acoustic attenuation; in addition, differences in grain size increases the acoustic wave dissipation.

5. Experimental validation

5.1. Frequency response function

The results obtained in the previous section can be used to experimental and numerically verify the approximated gradation profile for Young’s modulus; specifically, by calculating the resonance frequencies using a harmonic analysis. Particularly, the experimental and numerical Frequency Response Function (FRF) curves of Ni/Cu FGS are compared. For FGS case, the problem of how to calculate the experimental FRF curve arise; specifically, for small samples, the impact excitation and/or extraction methods by using modal parameters are difficult to be implemented [44]. The option to be used is inspired in the work of Skaf et al. [45].

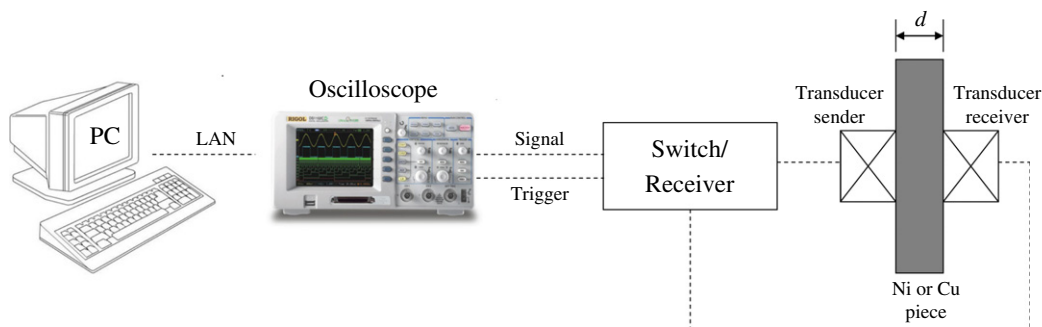


Fig. 11. Experimental setup for measuring the elastic properties by using ultrasound technique of non-FGS samples (considering only copper or nickel).

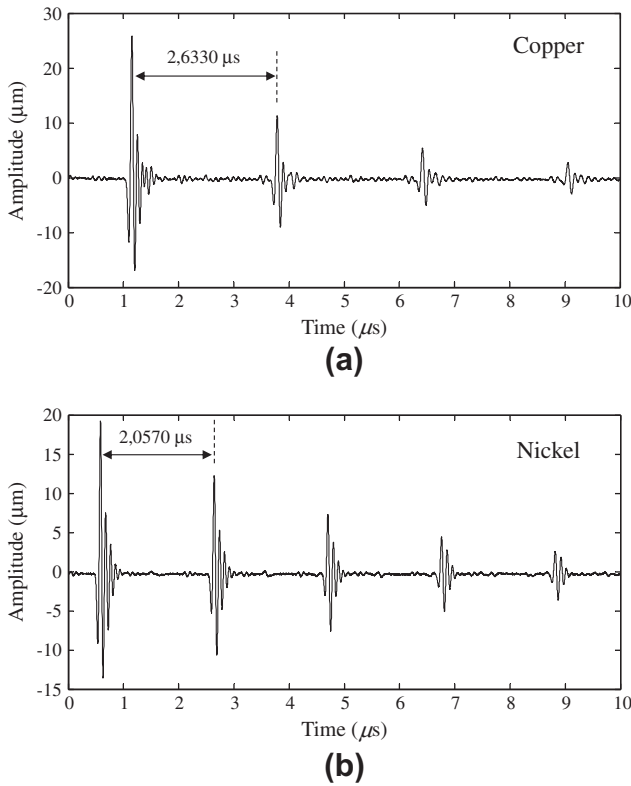


Fig. 12. Signals obtained from ultrasound test by using the experimental setup of Fig. 11 for homogeneous samples: (a) only copper (100% Cu); (b) only nickel (100% Ni).

Table 3
Young's modulus calculated by using ultrasonic test.

Datum	Non-FGS (only Cu)		Non-FGS (only Ni)	
	Sample 1	Sample 2	Sample 1	Sample 2
Thickness (mm) – d	6.051	5.993	5.887	5.964
Time peak-to-peak (μ s)	2.6330	2.6328	2.0570	2.0602
Longitudinal wave propagation velocity (m/s) – V_l	4596.3	4552.6	5723.9	5789.7
Poisson's ratio [42]	0.326	0.326	0.322	0.322
Young's modulus (GPa)	123.52	121.92	200.30	199.27

They use a combination of piezoelectric ceramic and non-piezoelectric structures for calculating the displacement FRF. The idea is to paste or embed a piezoelectric transducer in the studied structure and, by using an impedometer, to calculate the FRF. Skaf et al.

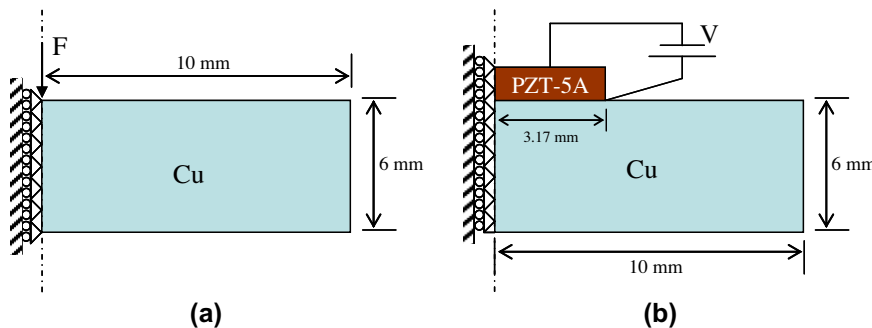


Fig. 13. Setup employed to calculate the simulated FRF of non-FGS by using piezoceramics: (a) model 1; (b) model 2.

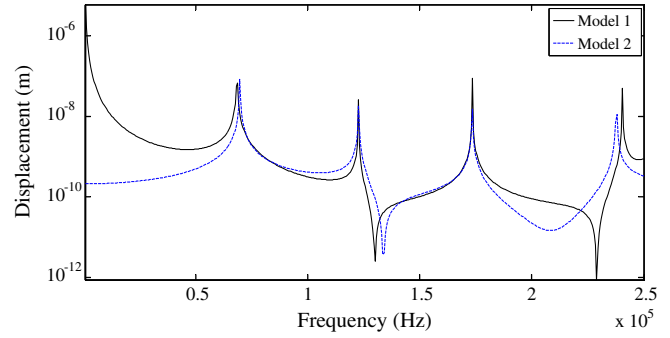


Fig. 14. Harmonic analysis curves by using the models of Fig. 13.

[45] conclude that, by using a piezoelectric ceramic of relatively small mass in relation to the non-piezoelectric structure, the first resonance frequencies can be determined with high accuracy.

In order to verify the above idea, several FE simulations are developed. Fig. 13a corresponds to the axisymmetric model of the non-piezoelectric structure that is analyzed experimentally (called model 1), considering only copper properties (in this case, a non-FGS is simulated). In this simulation case, the input excitation is a unit force applied to the middle of the structure. The approximated model (model 2) is presented in Fig. 13b, which consists of a piezoceramic bonded on the top and middle of the model 1. In model 2, the input is generated by applying a unit voltage in the piezoceramic.

To find the piezoelectric dimensions that best approximate the experimental FRF, several piezoceramic sizes are simulated by performing a harmonic analysis in ANSYSTM. In simulations, 6000 Q4 finite elements are employed. A commercially available PZT-5A piezoceramic with diameter of 6.35 mm and thickness of 0.378 mm acceptably approximates the FRF curve of model 1. This statement is corroborated by Fig. 14; in other words, dynamically, model 2 it behaves roughly as model 1. The difference between model 1 and 2, in the first four resonance frequencies, is less than 1.5%.

5.2. Experimental validation of FRF

Based on the previous results, a PZT-5A piezoelectric ceramic with a diameter of 6.35 mm and a thickness of 0.378 mm is bonded to a Ni/Cu FGS, which is fabricated by SPS technique. Subsequently, the resonance frequencies are found by using an impedance analyzer AGILENT 4194A. These frequencies are presented in Fig. 15. Same figure shows the FRF simulated curve of a Ni/Cu FGS, which is obtained considering the GFE formulation. In simulations, the following assumptions are taken:

- (i) The Young's modulus changes along the thickness following the curve of Fig. 10.

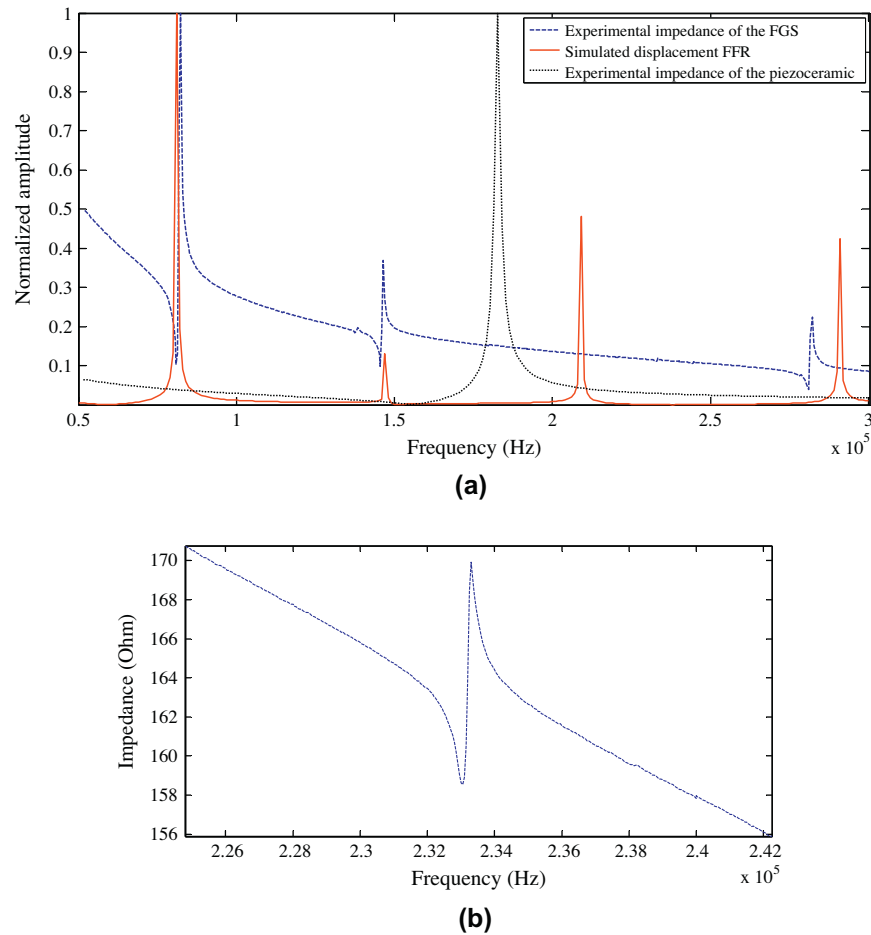


Fig. 15. Comparison of FRF curves for a Ni/Cu FGS sample: (a) experimental and simulated (by using GFE) impedance curves; (b) detail of impedance experimental curve at 225–242 kHz.

- (ii) The Young's modulus on the top and bottom surfaces is the mean of the values presented in Table 3: 122.72 GPa for copper and 199.78 GPa for nickel.
- (iii) The density and Poisson's modulus are kept constant along the thickness with values of 8625.8 kg/m³ and 0.324, respectively, which are the mean values presented in Table 2 (for density) and Table 3 (for Poisson's modulus).
- (iv) The Ni/Cu FGS is 19.95 mm in diameter and 5.96 mm in thickness.
- (v) The mesh has 70 × 40 finite elements.

In Fig. 15, although experimental and simulated vibration magnitudes are different, from both curves the resonance frequency values can be extracted. In experimental curve, these values correspond to peaks with electrical impedance tending to zero. In simulated curve, the resonance frequencies correspond to FRF peaks, which are presented in red and continuous line in Fig. 15a.

From Fig. 15 and Table 4 is observed that resonance frequency values of the first four modes, for experimental and simulated curve, are close. Beyond fourth vibration mode, the difference is increased, which is predictable from results presented in Fig. 14. Nevertheless, in the experimental curve, the vibration mode number 3 shows magnitude too small to be observed in plain view from Fig. 15a. In the simulated curve, this mode can be easily identified, as no damping is considered in harmonic analysis, which is detailed in Fig. 15b.

Additionally, Fig. 15a shows the experimental impedance curve of single piezoceramic, which is bonded to the FGS. As noted in the

Table 4

Resonance frequency obtained from curves of Fig. 15.

Vibration mode	Resonance frequency (kHz)		
	Simulated by GFE	Experimental	Difference (%)
Mode 1	81.00	80.97	0.04
Mode 2	147.00	145.58	0.96
Mode 3	209.00	233.05	−11.50
Mode 4	291.00	281.00	3.43

analyzed region (50–300 kHz), the resonance peak of single piezoceramic does not match any of the peaks of FGS curves, either simulated or experimental, and consequently, the curves in Fig. 15a represent the dynamic behavior of the FGS only.

Finally, Table 4 lists the first four resonance frequency values, both experimental and simulated values. The value of FGS simulated resonance frequency varies between 0.04% and 3.5% in relation to experimental value, except for vibration mode number 3, where the difference is 11.5%. The last difference probably is due to the influence of the vibration mode generated only by the single piezoceramic; specifically, at 182.7 kHz, which “moves” the FGS mode number 3 from expected position. Although these differences can be acceptable, also they are originated from several assumptions made during the simulation; for instance, uniform radial gradation, density and Poisson's modulus constants, and the use of mean values for Young's modulus on the top and bottom surfaces.

6. Conclusions

This work addresses the manufacturing and dynamic simulation of functionally graded structures (FGSs) made of Ni/Cu. For simulating these structures, a software is implemented, which allows the harmonic analysis of FGS by using the Graded Finite Element (GFE) formulation. In GFE, the material properties are interpolated inside each element, according to user-defined gradation function. Additionally, Ni/Cu FGS are manufactured by the technique of Spark Plasma Sintering (SPS), and they are characterized in terms of: (i) microstructure, by using a Scanning Electron Microscope (SEM); (ii) chemical composition; (iii) hardness test (Vickers); and (iv) elastic properties (by using ultrasonic testing) along the gradation direction. These characterization procedures demonstrate that a continuous property gradation is achieved along the thickness direction. Finally, experimental resonance frequencies of a Ni/Cu FGS sample are determined by using piezoceramics.

The following conclusions can be drawn:

- (i) By comparing the experimental and simulated resonance frequencies, it is observed that the GFE formulation approaches with great accuracy the resonance frequencies obtained experimentally; specifically, difference smaller than 1% are obtained, at the first two vibration modes. However, the difference increases when higher order vibration modes are considered; thus, at the fourth mode, the difference between the simulated and experimental response is approximately 3.5%.
- (ii) Moreover, by using the hardness variation curve along the gradation direction, an appropriate approach to measure gradation variation is obtained. This assumption is advantageous, as the hardness calculation is a simple procedure, which requires a simplified sample preparation. Otherwise, for determining the gradation curve, we should manufacture and characterize a homogeneous structure with the approximate composition of each green layer; thus, for the Ni/Cu FGS samples here considered, six homogeneous structures should be manufactured, each with the same composition of each green layer in Fig. 4. In addition, the elastic properties for each one should be determined. Nevertheless, the use of hardness curve for approximating the gradation function of elastic properties can only be considered if the materials are isotropic and completely solid miscible. Accordingly, as future work, further studies in this direction should be developed.

Acknowledgments

The first author thanks FAPESP (São Paulo State Foundation Research Agency) for supporting him in his graduate studies through the fellowship No. 05/01762-5. The second author's contribution was based on work supported by the USA National Science Foundation (NSF), while working at the foundation as a program director. The last author is thankful for the financial support received from both CNPq (National Council for Research and Development, Brazil, No. 303689/2009-9) and FAPESP (Process No. 2011/02387-4). Finally, we are grateful to Dr. Mario Gonzalez Ramirez at Department of Material and Metallurgical engineering from University of São Paulo for his technical support in order to obtain the microphotographs of FGS samples and their chemical composition by using Energy Dispersive Spectrometry.

References

- [1] Aboudi J, Pindera MJ, Arnold SM. Higher-order theory for functionally graded materials. *Compos Part B – Eng* 1999;30:777–832.

- [2] Kieback B, Neubrand A, Riedel H. Processing techniques for functionally graded materials. *Mater Sci Eng A* 2003;362:81–105.
- [3] Reiter T, Dvorak GJ, Tvergaard V. Micromechanical models for graded composite materials. *J Mech Phys Solids* 1997;45:1281–302.
- [4] Yin HM, Sun LZ, Paulino GH. Micromechanics-based elastic model for functionally graded materials with particle interactions. *Acta Mater* 2004;52:3535–43.
- [5] Koizumi M. FGM activities in Japan. *Compos Part B: Eng* 1997;28:1–4.
- [6] Embury JD, Freund LB, Needleman A, Shih CF, Spaepen F, Suresh S. Summary. *J Mech Phys Solids* 1996;44:823–5.
- [7] Yu MH, Zhou B, Bi DB, Shaw D. Preparation of graded multilayer materials and evaluation of residual stresses. *Mater Des* 2010;31:2478–82.
- [8] Chiu T-C, Erdogan F. One-dimensional wave propagation in a functionally graded elastic medium. *J Sound Vib* 1999;222:453–87.
- [9] Asghari M, Ahmadian MT, Kahrobaian MH, Rahaeifard M. On the size-dependent behavior of functionally graded micro-beams. *Mater Des* 2010;31:2324–9.
- [10] Pindera M-J, Aboudi J, Arnold SM. Limitations of the uncoupled, RVE-based micromechanical approach in the analysis of functionally graded composites. *Mech Mater* 1999;20:77–94.
- [11] Hashin Z. Analysis of composite materials, a survey. *J Appl Mech* 1983;50:481–505.
- [12] Praveen GN, Reddy JN. Nonlinear transient thermoelastic analysis of functionally graded ceramic-metal plates. *Int J Solids Struct* 1998;35:4457–76.
- [13] Reddy JN. Analysis of functionally graded plates. *Int J Numer Methods Eng* 2000;47:663–84.
- [14] Chakraborty A, Gopalakrishnan S, Kausel E. Wave propagation analysis in inhomogeneous piezo-composite layer by the thin layer method. *Int J Numer Methods Eng* 2005;64:567–98.
- [15] Chakraborty A, Gopalakrishnan S. A spectral formulated finite element for wave propagation analysis in functionally graded beams. *Int J Solids Struct* 2003;40:2421–48.
- [16] Banks-Sills L, Eliasi R, Berlin Y. Modeling of functionally graded materials in dynamic analyses. *Compos Part B: Eng* 2002;33:7–15.
- [17] Rubio WM, Buiochi F, Adamowski JC, Silva ECN. Modelling of functionally graded piezoelectric ultrasonic transducers. *Ultrasonics* 2009;49:484–94.
- [18] Kim JH, Paulino GH. Isoparametric graded finite elements for nonhomogeneous isotropic and orthotropic materials. *J Appl Mech-Trans ASME* 2002;69:502–14.
- [19] Santare MH, Lambros J. Use of graded finite elements to model the behavior of nonhomogeneous materials. *J Appl Mech* 2000;67:819–22.
- [20] Rubio WM, Paulino GH, Silva ECN. Tailoring vibration mode shapes using topology optimization and functionally graded material concepts. *Smart Mater Struct* 2011;20:025009.
- [21] Santare MH, Thamburaj P, Gazona GA. The effect of graded strength on damage propagation in continuously nonhomogeneous materials. *J Eng Mater Technol* 2003;125:412–7.
- [22] Zhang Z, Paulino GH. Wave propagation and dynamic analysis of smoothly graded heterogeneous continua using graded finite elements. *Int J Solids Struct* 2007;44:3601–26.
- [23] Silva ECN, Carbonari RC, Paulino GH. On graded elements for multiphysics applications. *Smart Mater Struct* 2007;16:2408–28.
- [24] Parameswaran V, Shukla A. Dynamic fracture of a functionally graded material having discrete property gradation. *J Mater Sci* 1998;33:3303–11.
- [25] Parameswaran V, Shukla A. Processing and characterization of a model functionally graded material. *J Mater Sci* 2000;35:21–9.
- [26] Rousseau C-E, Tippur HV. Influence of elastic variations on crack initiation in functionally graded glass-filled epoxy. *Eng Fract Mech* 2002;69:1679–93.
- [27] Wattanasakulpong N, Prusty BG, Kelly DW, Hoffman M. Free vibration analysis of layered functionally graded beams with experimental validation. *Mater Des* 2012;36:182–90.
- [28] Winter A, Corff B, Reimanis I, Rabin B. Fabrication of graded nickel-alumina composites with a thermal-behavior-matching process. *J Am Ceram Soc* 2004;83:2147–54.
- [29] Lin X, Yue T, Yang H, Huang W. Phase evolution in laser rapid forming of compositionally graded Ti–Ni alloys. *J Eng Mater Technol* 2009;131:1–5.
- [30] Zienkiewicz OC, Taylor RL. The finite element method. 4th ed. London, New York: McGraw-Hill; 1991.
- [31] Munir ZA, Anselmi-tamburini U, Ohyanagi M. The effect of electric field and pressure on the synthesis and consolidation of materials: a review of the spark plasma sintering method. *J Mater Sci* 2006;41:763–77.
- [32] Tokita M. Mechanism of Spark Plasma Sintering (SPS). In: Proceedings of 2000 powder metallurgy world congress; 2000. p. 729–32.
- [33] Zhang Z-H, Wang F-C, Wang L, Li S-K. Ultrafine-grained copper prepared by spark plasma sintering process. *Mater Sci Eng A* 2008;476:201–5.
- [34] Zhang Z-H, Wang F-C, Wang L, Li S-K, Shen M, Osamu S. Microstructural characteristics of large-scale ultrafine-grained copper. *Mater Charact* 2008;59:329–33.
- [35] Yao X, Huang Z, Cheng L, Jiang D, Tan S, Michel D, et al. Alumina-nickel composites densified by spark plasma sintering. *Mater Lett* 2005;59:2314–8.
- [36] Grieken RV, Markowicz A, Török S. Energy-dispersive X-ray spectrometry: present state and trends. *Fresen J Anal Chem* 1986;324:825–31.
- [37] ASTM Standard E384–09. Standard test method for microindentation hardness of materials. West Conshohocken, PA: ASTM International; 2003.

- [38] Oliver WC, Pharr GM. Measurement of hardness and elastic modulus by instrumented indentation: advances in understanding and refinements to methodology. *Mater Res Soc* 2004;19:3–20.
- [39] Meza J, Franco E, Farias M, Buiocchi F, Souza M, Cruz J. Medición del módulo de elasticidad en materiales de ingeniería utilizando La técnica de indentación instrumentada y de ultrasonido. *Revista de Metalurgia* 2008; 44:52–65.
- [40] Lawn BR, Howes VR. Elastic recovery at hardness indentations. *J Mater Sci* 1981;16:2745–52.
- [41] Marshall DB, Noma T, Evans AG. A simple method for determining elastic modulus to hardness ratios using Knoop indentation. *Int J Am Ceram Soc* 1982;65:c175–6.
- [42] Beaton CF, Hewitt GF, Liley PE. *Physical property data for the design engineer*. New York: Hemisphere Publishing Corporation; 1989.
- [43] Kino G. *Acoustic waves: devices, imaging, and analog signal processing*. Corrected ed. New Jersey: Prentice-Hall, Inc.; 2000.
- [44] Ewins DJ. *Modal testing: theory and practice*. England: Research Studies Press; 1988.
- [45] Skaf A, Nassar F, Lefebvre B, Nongaillard B. A new acoustic technique to monitor bread dough during the fermentation phase. *J Food Eng* 2009;93:365–78.
- [46] Rubio WM. *Otimização topológica de transdutores piezelétricos com gradação funcional de material: projeto, simulação, análise e fabricação*. PhD thesis, University of São Paulo; 2010.